

Evaluation of acoustic emission source localization accuracy in concrete structures

Zhang, Fengqiao; Pahlavan, Lotfollah; Yang, Yuguang

DOI

[10.1177/1475921720915625](https://doi.org/10.1177/1475921720915625)

Publication date

2020

Document Version

Final published version

Published in

Structural Health Monitoring

Citation (APA)

Zhang, F., Pahlavan, L., & Yang, Y. (2020). Evaluation of acoustic emission source localization accuracy in concrete structures. *Structural Health Monitoring*, 19(6), 2063-2074.
<https://doi.org/10.1177/1475921720915625>

Important note

To cite this publication, please use the final published version (if applicable).
Please check the document version above.

Copyright

Other than for strictly personal use, it is not permitted to download, forward or distribute the text or part of it, without the consent of the author(s) and/or copyright holder(s), unless the work is under an open content license such as Creative Commons.

Takedown policy

Please contact us and provide details if you believe this document breaches copyrights.
We will remove access to the work immediately and investigate your claim.

Evaluation of acoustic emission source localization accuracy in concrete structures

Structural Health Monitoring

1–12

© The Author(s) 2020

Article reuse guidelines:

sagepub.com/journals-permissions

DOI: 10.1177/1475921720915625

journals.sagepub.com/home/shm

Fengqiao Zhang¹ , Lotfollah Pahlavan² and Yuguang Yang¹

Abstract

Acoustic emission source localization is a promising monitoring technique for concrete structures. However, the accuracy of acoustic emission source localization is influenced by many factors, such as the presence of cracks, which are commonly observed in existing reinforced concrete structures. In this article, the acoustic emission source localization is evaluated using a numerical model with a total number of 11,827,200 independent simulated tests. In this work, the investigated influential factors include the presence of cracks, arrival time picking error, and sensor layout. The accuracy of source localization is quantified by the characteristic error defined in this article. Using the proposed wave propagation properties, a relatively stable characteristic error of 150 mm is estimated in the detection zone with the maximum sensor spacing less than 1 m. The evaluation approach and simulated characteristic error are validated experimentally by comparing the 200 manually generated signals using hammer hits on a cracked concrete beam.

Keywords

Acoustic emission source localization, concrete structures, crack, arrival time picking error, accuracy

Introduction

Acoustic emission (AE) technique shows promising features in detecting damages, such as crack opening/closure^{1,2} and de-bonding of reinforcement,³ in concrete structures. Damage is generally caused by irreversible localized structural changes, which emit elastic waves inside the material. The location of these changes can be traced back using different arrival times of the same wave signal at different locations with multiple sensors. The process is called AE source localization.⁴ This technique turns out to be efficient in detecting damages in metal structures due to the homogeneity of the medium.⁵ However, for many reinforced concrete structures, especially existing concrete structures, the arrival times of waves are influenced by the presence of cracks.⁶ A generic methodology to evaluate the accuracy of applying the traditional localization method, which is based on the assumption of constant wave velocity inside the concrete structures, is necessary. In order to verify the accuracy of the source localization, various methods have been introduced in the literature. Schechinger and Vogel⁷ approached experimentally by locating AE from cracking. The comparison with the real crack pattern indicated the source localization accuracy qualitatively. Tsangouri et al.⁸ assessed the

source localization accuracy by locating an embedded transducer inside concrete with known position. The accuracy of the source localization was quantitatively described by the ratio between the spatial error and sensor spacing. Zhang⁹ approached numerically by locating the simulated sources in a modeled concrete beam. The source localization accuracy was quantified by the spatial localization error. The inconsistent way of evaluation causes vague understanding of the source localization accuracy. A more consistent manner of evaluation is needed to assess the accuracy of the AE source localization in concrete structures.

The aim of this article is to evaluate the accuracy of AE source localization in concrete structures in a consistent manner and evaluate the effect of possible influencing factors. To do so, numerical models which simulate AE measurement on a hypothetical concrete

¹Department of Engineering Structures, Delft University of Technology, Delft, The Netherlands

²Department of Maritime and Transport Technology, Delft University of Technology, Delft, The Netherlands

Corresponding author:

Fengqiao Zhang, Department of Engineering Structures, Delft University of Technology, Stevinweg 1, 2628 CN Delft, The Netherlands.

Email: F.Zhang-5@tudelft.nl

beam with different crack configurations and sensor layouts are developed. Factors that may influence the source localization results include the position and the height of cracks, arrival time picking error, and sensor layout. The accuracy of AE source localization is quantified by the term characteristic localization error e_{ck} . The evaluation approach and the numerically derived e_{ck} are then validated experimentally by comparing the manually generated signals using hammer hits with the known locations.

AE source localization and error study

AE source localization technique

Triangulation technique¹⁰ is a widely applied method for AE source localization. The algorithm assumes a constant wave velocity in the medium. For more advanced algorithms taking into account variable wave velocity distribution, studies reported in Shiotani et al.¹¹ and Pahlavan et al.¹² are referred to, which will not be discussed further in the study.

Suppose that an AE event is captured by sensors at different locations with corresponding arrival times of waves, the difference between the travel distances from the source to two arbitrary sensors is expected as

$$\|\mathbf{x}_S - \mathbf{x}_{R,i}\| - \|\mathbf{x}_S - \mathbf{x}_{R,j}\| = c \cdot (t_i - t_j), \forall i, j \in [1, 2, \dots, N] \quad (1)$$

where \mathbf{x}_S is the spatial coordinates of the AE event; N is the number of sensors that can receive the waves; $\mathbf{x}_{R,i}$ and $\mathbf{x}_{R,j}$ are the spatial coordinates of sensors i and j , respectively; t_i and t_j are the arrival times of waves at sensors i and j , respectively; and c is the assumed wave velocity.

In this study, the grid search method⁴ is employed. The measured volume is discretized by a grid of possible source locations (referred as grid search zone). The source location is estimated by searching the grid point which has the minimal residual between the calculated and the measured distance difference from available sensor pairs

$$r(\mathbf{x}_S) = \sum_{i=1}^{N-1} \sum_{j=i+1}^N [|\|\mathbf{x}_S - \mathbf{x}_{R,i}\| - \|\mathbf{x}_S - \mathbf{x}_{R,j}\|| - c \cdot (t_i - t_j)]^2 \quad (2)$$

An illustration of the source location estimation from the minimal residual in the grid search zone is shown in Figure 1(a). However, the minimal residual in the grid search zone might not be the global minimum in the infinite space. One of the consequences is estimating the source location on the edge of the grid search zone which is further away from the minimum

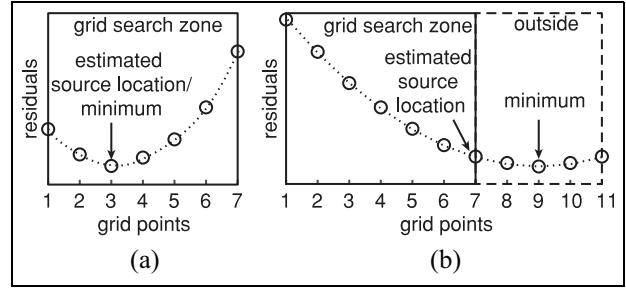


Figure 1. Estimated source location: (a) in the inner part of the grid search zone and (b) on the edge of the grid search zone.

(Figure 1(b)). Those source localization results on the edge of the grid search zone are considered to be not reliable and filtered out in this article.

Localization error

In the described source localization procedure, arrival times and sensor layout are the two main parameters for the triangulation method. Factors that may influence these inputs are considered to be the sources of localization errors in this study. They are as follows:

- Arrival time picking method, which is regarded as a systematic error;
- Cracks through the wave travel path, which is from the concrete structure;
- Sensor layout, which on one hand determines the detective capability. Sources outside the sensor enclosed zone could not be located accurately. On the other hand, sensor layout influences attenuation of the wave signal. Too large attenuation of the signal results in missing of AE events or increased errors since less sensors are utilized in the localization procedure.

For arrival time picking method, the widely used methods are fixed or floating thresholds that are implemented in the acquisition system.^{13,14} The arrival times are decided by the first point that crosses a threshold which is either a fixed value or a floating value relating to the signal amplitude. Schechinger and Vogel⁷ quantified the picking error of the floating threshold method by comparing the automatic pickings with the manual pickings. They found that 27.1% of the results had errors less than 1.25 μ s, 20.2% between 1.25 and 2.5 μ s, 24.2% between 2.5 and 7.5 μ s, and the rest were considered not good. Since signals have different signal-to-noise ratios, it is more likely to have larger errors when fixed threshold method is used.

The presence of cracks delays the arrival times due to two possible effects: the reduction of the wave

velocity at the region close to the crack or the diffraction of the wave at the crack tip, which will be further discussed in section “Wave propagation in concrete structures.”

For sensors that can capture the AE event, the two sources of errors, which are the arrival time picking method and the presence of cracks, are independent to each other, therefore can be superimposed, resulting in the influenced (actual) arrival times

$$t_i^* = t_i + \Delta t_{pk,i} + \Delta t_{cr,i}, \forall i \in [1, 2, \dots, N] \quad (3)$$

where t_i is the expected arrival time at sensor i in sound concrete, $\Delta t_{pk,i}$ is the arrival time picking error at sensor i , and $\Delta t_{cr,i}$ is the arrival time delay due to the presence of a crack at sensor i .

By plugging the influenced arrival times in equation (2), a possibly erroneous source location is calculated. The localization error is defined as the distance between the actual source location and the estimated source location

$$error = \|\mathbf{x}_S - \mathbf{x}_S^*\| \quad (4)$$

where \mathbf{x}_S^* is the estimated spatial coordinates of the AE event.

In addition, the presence of steel reinforcements may influence the arrival times due to the local change of wave speed and scattering. Simulations showed an arrival time delay of less than 5 μ s.⁷ This value may change with dimensions of steel and wave length. It is a complex phenomenon to model. This article does not involve the influence of steel tendon on the source localization. But with the same approach described above, the influence of steel tendon can be included by adding the corresponding arrival time delays in equation (3).

Wave propagation in concrete structures

In concrete structures, the AE signals can experience extraordinary complications on their way from the source to the sensors. Most AE source localization methods including the one adopted in this article only take into account the first arrival of the signals. Thus, proper understanding of the properties of the first arrival part of a wave signal in terms of travel time and amplitude is essential for the analysis of source localization in this study.

In sound concrete, the wave travel paths are assumed to be straight. Waves that travel from the source location of an AE event denoted by \mathbf{x}_S to the location of the sensor (receiver) i are denoted by $\mathbf{x}_{R,i}$ with an arrival time expressed by

$$t_i = t_0 + \frac{\|\mathbf{x}_S - \mathbf{x}_{R,i}\|}{c_P} \quad (5)$$

where c_P is the P-wave velocity (around 4100 m/s in concrete from former tests⁶) and t_0 is the onset time of the AE event.

The attenuation of the first arrival P-waves in sound concrete generally comes from two sources: the material attenuation and the spherical spreading loss.⁹ The decibel value of the amplitude of the signal arrived at the location of sensor i is

$$A_i = A_0 - 20 \log_{10} \left(\frac{r}{\|\mathbf{x}_S - \mathbf{x}_{R,i}\|} \right) - \alpha_m \cdot \|\mathbf{x}_S - \mathbf{x}_{R,i}\| \quad (6)$$

where A_0 is the amplitude in dB of the source pulse; r is the source sphere radius; and α_m is the material attenuation factor, which is related to the implemented frequency¹⁵ (around 20 dB/m at frequency around 60 kHz for concrete from former research⁹).

When a crack lies between the AE source and the sensor, the first arrival wave may be from one of the two alternatives: (1) waves go through the crack (referred as direct waves) or (2) waves diffracted by the crack tip (referred as tip-diffracted waves), shown in Figure 2.

Generally, the waves which arrive earlier but not yet attenuate below the threshold of the sensor are recognized as the first arrival waves. Hence, the two criteria to determine the first arrival are (1) the arrival time and (2) the amplitude. For tip-diffracted waves, the influence of the crack tip on the amplitude and phase change¹⁶ were neglected in this study with the assumption that the crack tip only changes the wave travel direction. The arrival time and the amplitude of the tip-diffracted waves were estimated using equations (5) and (6) with a travel distance of $\|\mathbf{x}_S - \mathbf{x}_{cr,i}\| + \|\mathbf{x}_{cr,i} - \mathbf{x}_{R,i}\|$, where $\mathbf{x}_{cr,i}$ is the location of the wave diffraction point (crack tip in Figure 1). For direct waves through a crack (Figure 3(c)),⁶ a study was reported on the influence of a relaxed crack (the load which causes the crack is removed) with surface opening in the range of [0.05, 3] mm. The study showed that a relaxed crack causes a delay between 5 and 20 μ s depending on the angle between the wave propagating direction and the crack (see Figure 3(b)).⁶ This angle dependence relation of the elastic waves with respect to a crack band turns out

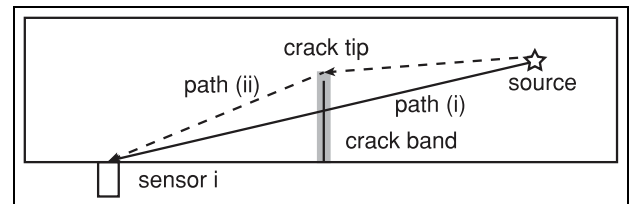


Figure 2. Wave propagation in existing concrete structures with a crack between the source and the sensor.

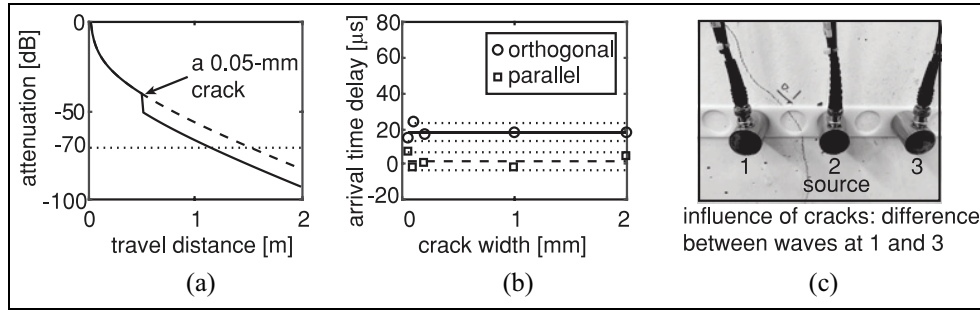


Figure 3. (a) Amplitude attenuation, (b) arrival time delay in travel distance of 80 mm orthogonal and parallel to the crack, and (c) test setup to study crack effect.⁶

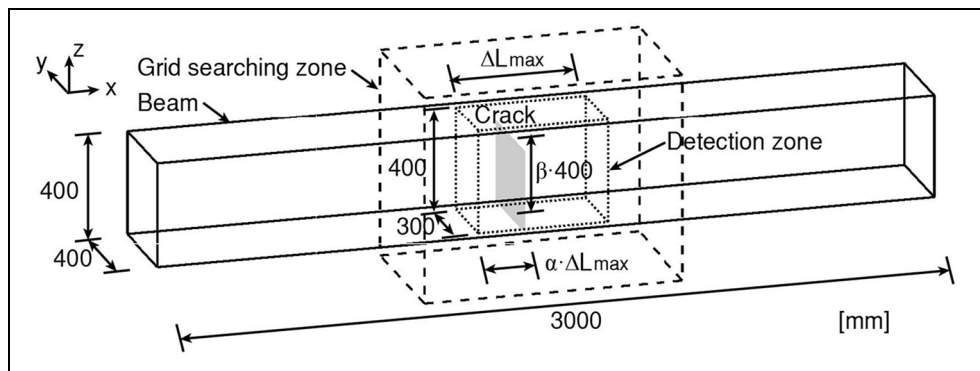


Figure 4. Beam configuration, detection zone, and grid searching zone.

to be rather complex, no theoretical model is available in the literature yet. We consider an elliptical distribution of the wave speed in the crack band. The surface opening of the crack seems to have limited influence on the travel time delay in the measured range. For the amplitude of the waves, the tested cracks in the range of [0.05, 3] mm caused an additional amplitude drop from -10 to -50 dB.¹⁷ Combined with the material attenuation and the spherical spreading loss in equation (6), the attenuation of the direct waves ($\Delta A = A_i - A_0$) with a 0.05-mm crack at 0.5 m away from the source is illustrated in Figure 3.

Simulation of AE source localization in a concrete beam with a flexural crack

A reliable evaluation of the AE source localization in concrete structures, considering the discussed influential factors of the presence of cracks, accuracy of arrival time picking, and sensor layout, requires large quantity of measurements, which is costly and labor-intensive. Besides, in a three-dimensional (3D) measurement, it is generally not feasible to manually and non-intrusively excite a source pulse inside the structure

at a predefined position for calibration. Therefore, a more practical option is to simulate the AE source localization process including the possible influential factors based on realistic concrete structures using a numerical model. The source localization errors discussed previously are investigated with the model.

The reference model of this study is a concrete beam with a relaxed crack (Figure 4). The dimension of the beam is 3000 mm \times 400 mm \times 400 mm. The wave speed of the first arrivals in the sound concrete is obtained through previous experiments being 4100 m/s, and the material attenuation factor is 20 dB/m for signals with frequency centered at 60 kHz. The crack is a typical flexural crack with a surface crack width of 0.05 mm, which propagated from the bottom of the beam and stopped at a certain height of the beam due to force equilibrium along the cross section.¹⁷ The variation of the crack surface at aggregate level is neglected resulting in a plain surface being perpendicular to the longitudinal direction of the beam.

Four AE sensors with central frequency of 60 kHz are applied on the surface of the beam around the crack. Sensors are arranged in eight different sensor layouts, which can be categorized in four groups: in

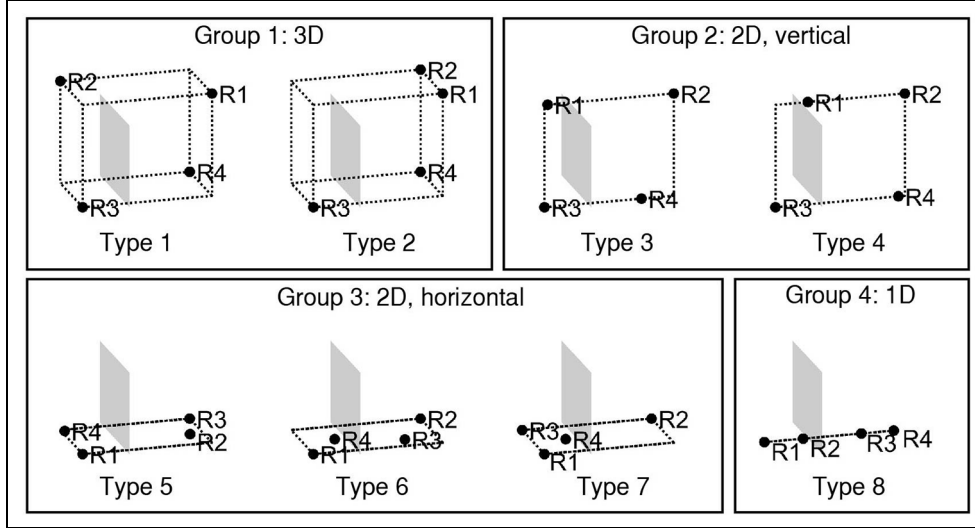


Figure 5. Sensor layouts (R1-4) and detection zone (enclosed by dashed lines) in four groups: 3D, 2D vertical, 2D horizontal, and 1D.

3D, 2D vertical, 2D horizontal, and 1D (Figure 5). Sensor layouts on the vertical cross section (Group 2) and on the bottom surface (Group 3) are included to simulate the practical cases, when only the side surface or the bottom surface is accessible. Sensor layout of 1D (Group 4) is included to simulate slender structures where only 1D measurement is necessary. Since AE source localization cannot give reliable estimation of the locations of the sources outside the sensor covering zone,¹⁷ the detection zone is defined as the sensor covering zone, which is in a volume, a plane, or a line, when the sensor layout is 3D, 2D, or 1D, respectively (indicated by dashed lines in Figure 5(a)). The studied sensor layouts are considered comparable as they share the same length (for all groups), width (for Group 1 and Group 3), or height (for Group 1 and Group 2).

In this model, the maximum sensor spacing in x -direction (see Figure 4 for the directions) can be adjusted to study the influence of wave travel distance on the accuracy of source localization. Since stress state of the beam is plain stress, the crack distribution in y -direction is assumed to be constant. The position of the crack in x -direction and the height of the crack tip in the detection zone are adjustable and evaluated by (indicated in Figure 4)

$$\begin{aligned} \alpha &= \frac{\Delta L_{x, \max}}{l_{x, cr}} \\ \beta &= \frac{\Delta L_{z, \max}}{l_{z, cr}} \end{aligned} \quad (7)$$

where $l_{x, cr}$ is the distance from the left edge of the detection zone to the middle of the crack profile in x -direction, $l_{z, cr}$ is the distance from the bottom of the detection zone to the crack tip in z -direction, $\Delta L_{x, \max}$ is

the maximum sensor spacing in x -direction, $\Delta L_{z, \max}$ is the maximum sensor spacing in z -direction, α is the crack position factor, and β is the crack height factor.

For a crack whose middle is 250 mm to the left edge and tip reaches 320 mm in a detection zone with 1000 mm length and 400 mm height, α and β values are then 0.25 and 0.8, respectively.

Twenty-four independent models with eight sensor layouts were built (listed in Table 1). In each model, a total number of 308 ($11 \times 4 \times 7$) assumed possible source locations were uniformly distributed in the volume $\Delta L_{x, \max} \times 300 \text{ mm} \times 400 \text{ mm}$. A source pulse with amplitude of 100 dB was generated at each source location in turn. Assuming a noise level of less than 30 dB, the threshold of the sensors was set to be constant at 30 dB. The influence of the crack on the wave propagation followed the description in section “Wave propagation in concrete structures.” From Figure 3(a), the attenuation of a wave when it travels through a crack and 1 m distance was larger than 70 dB. Such a wave would be filtered by the constant threshold. Instead, the tip-diffracted waves were received.

The arrival time picking error was assumed to be a uniform random variable with a range of $[0, 5] \mu\text{s}$. The influenced arrival times, determined with equation (3), were used to estimate the source location with the grid search method outlined in section “AE source localization technique.” The grid searching zone was set to be $2\Delta L_{x, \max} \times 600 \text{ mm} \times 800 \text{ mm}$ with a grid size of 10 mm. The calculated 3D source localization error was then projected to the detection zone. This procedure was repeated 200 times for each source. In the end, a total number of 11,827,200 ($24 \times 8 \times 308 \times 200$) independent realizations were generated to evaluate the source localization error.

Table 1. Configurations and characteristic source localization error in sensor layout Type 1 (see Figure 4).

Configuration No.	$\Delta L_{x, \max}$ (mm)	α	β	Characteristic error e_{ck} in sensor layout Type 1 (mm) ^a
1	300	0.33	0.8	154.42
2	500	0.13	0.8	150.67
3	500	0.17	0.8	151.91
4	500	0.20	0.8	155.60
5	500	0.25	0.8	158.11
6	500	0.33	0.8	160.45
7	500	0.40	0.8	164.92
8	500	0.50	0.8	164.86
9	500	0.60	0.8	164.86
10	500	0.67	0.8	160.62
11	500	0.75	0.8	158.04
12	500	0.80	0.8	155.81
13	500	0.83	0.8	151.91
14	500	0.88	0.8	149.70
15	500	0.33	0	23.33
16	500	0.33	0.1	75.79
17	500	0.33	0.2	101.21
18	500	0.33	0.4	143.80
19	500	0.33	0.6	155.49
20	500	0.33	1	152.35
21	800	0.33	0.8	173.78
22	1000	0.33	0.8	160.35
23	1200	0.33	0.8	145.64
24	1500	0.33	0.8	145.53

^aIn each configuration, eight types of sensor layouts are tested, with the results in sensor layout Type 1 listed.

For each type of sensor layout, the characteristic source localization error e_{ck} was defined as the error above which not more than 5% of the realizations are expected. e_{ck} was used to quantify the accuracy of source localization. The value of 5% is a typically used significance level in civil engineering practice¹⁸ (with a confidence level of $0.95 = 1 - 0.05$). Larger characteristic error was expected when the significance level was lowered. To verify the influence of significance level, we compared the characteristic error with significance levels of 5% and 1% in one test configuration. The selection of the significance level depends on the requirement of the study. In this article, we used the characteristic error with significance level of 5%. The notation e_{ck} in this article without specific notes indicates the characteristic error with significance level of 5%. The notation $e_{ck,0.01}$ indicates the characteristic error with significance level of 1%.

Results

The source localization results of the test configuration 22 in Table 1 with $\Delta L_{x, \max} = 1000$ mm, $\alpha = 0.33$, and $\beta = 0.8$ in sensor layout Type 1 is shown in Figure 6 as

an example. The error lines start from the actual source locations and end at the estimated source locations with cross markers.

The source localization results on the edge of the grid searching zone (in gray) were considered not to be reliable, thus filtered out according to section “AE source localization technique.” In Type 1, around 73% of the source localization results remained. In other types of sensor layouts, around 83% (Type 2), 66% (Type 3), 71% (Type 4), 75% (Type 5), 74% (Type 6), 83% (Type 7), and 73% (Type 8) remained.

The remaining source localization results in the sensor layouts of different dimensions (3D, 2D, and 1D) were compared by projecting to the relative detection zones of the sensor layouts. A projection example in sensor layout Type 1 (Group 1), Type 3 (Group 2), Type 5 (Group 3), and Type 8 (Group 4) is shown in Figure 7. The dot lines enclose the detection zones which are of 3D, 2D vertical, 2D horizontal, and 1D, respectively. The “+” mark indicates the real source location, and the “×” mark indicates the estimated source location. The source localization results in 2D sensor layouts (in x - y plane) were dominated by error component in z -direction. Similarly, the source localization results in 1D sensor layout (in x -axis) had larger errors in y - and z -direction. This was expected since triangulation technique could not locate accurately in the dimensions not covered by the detection zone. Therefore, the source localization results were projected to the detection zone by eliminating the error components in other dimensions. For example, in Type 5 present in Figure 7, only errors in x - y plane were considered. After projection, the source localization errors of the four sensor layouts were comparable, being 43.33, 50.11, 44.72, and 40 mm, respectively.

The source localization results of the 200 repeated tests were assumed to follow a normal distribution. Student’s t -test¹⁹ proved the assumption of normal distribution with a significance level lower than 0.01. The cumulative distribution function (CDF) of the source localization errors for each type of sensor layout is shown in Figure 8. The value of e_{ck} in the test configuration 22 for the eight sensor layouts were 160.35 mm (Type 1), 172.76 mm (Type 2), 115.95 mm (Type 3), 116.62 mm (Type 4), 117.04 mm (Type 5), 130 mm (Type 6), 150.33 mm (Type 7), and 55 mm (Type 8). Generally, 3D sensor layouts had larger e_{ck} , which was expected, since the errors in the 3D layout were the original errors without elimination of the error components (projection to the detection zone). The source localization in the 1D sensor layout had the smallest error of 55 mm, where only the x -components were considered.

In this test configuration, $e_{ck,0.01}$ was computed and compared with e_{ck} . Figure 8 shows that characteristic

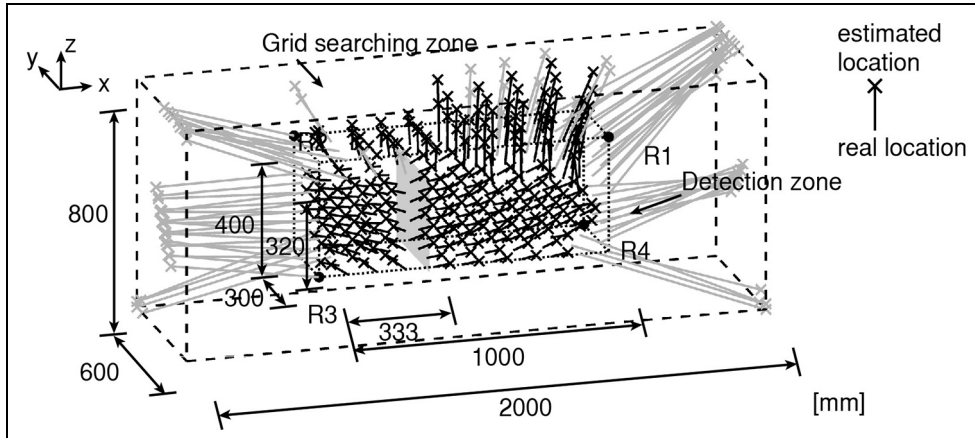


Figure 6. Source localization results of test configuration 22, layout Type I.

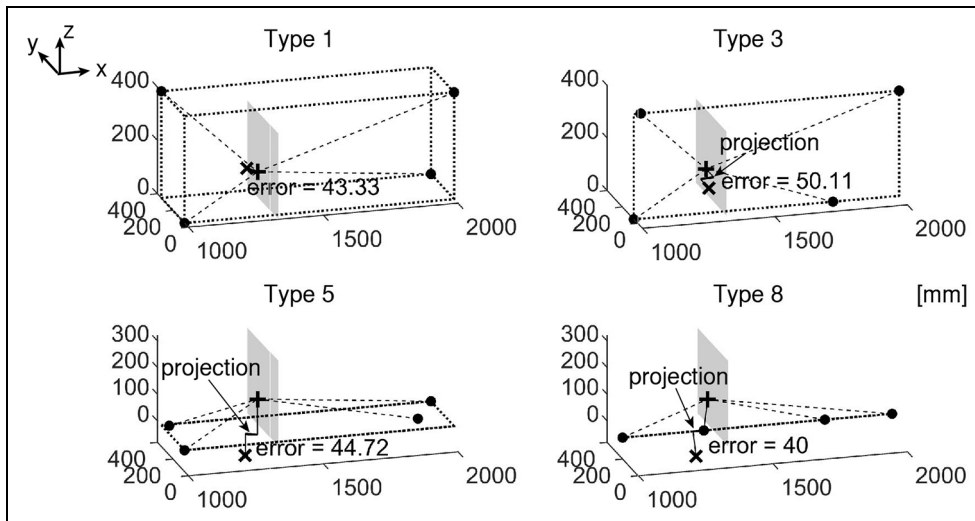


Figure 7. Source localization results of the source at (1300, 150, 133.3) mm of test configuration 22, in sensor layouts: Type 1, Type 3, Type 5, and Type 8.

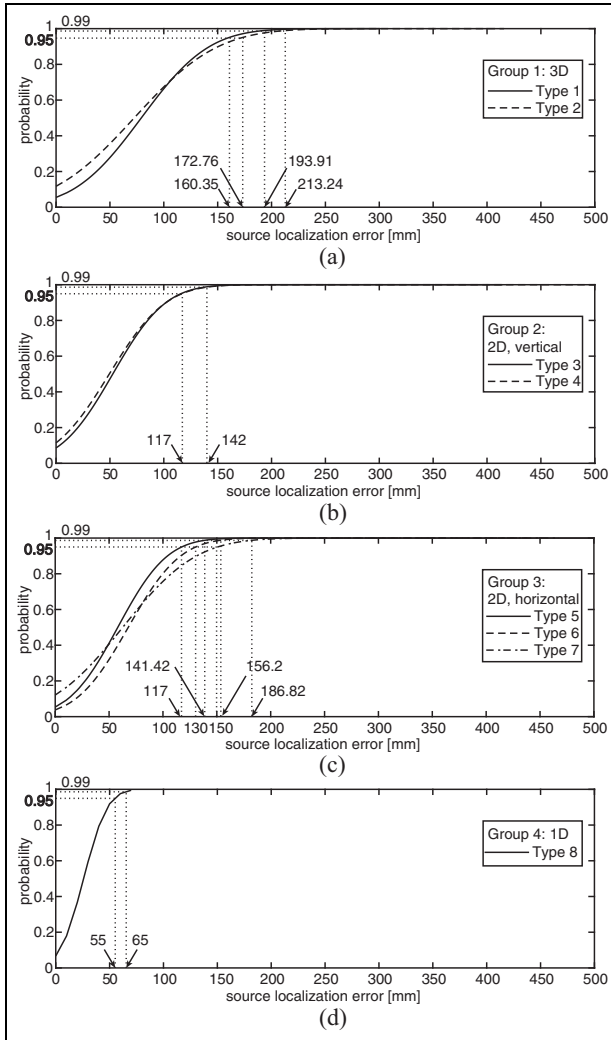
error increased when more realizations were expected to have errors less than the characteristic error. Table 2 compares e_{ck} and $e_{ck,0.01}$. The increase in characteristic error in each type of sensor layout due to the decrease in significance level was between 18.2% and 24.3%.

The above-introduced analysis procedure was implemented on all the designated configurations listed in Table 1. The characteristic errors e_{ck} with different $\Delta L_{x, \max}$ (test configurations 1, 6, 21, 22, 23, and 24) is shown in left column of Figure 9. The compared configurations had constant α of 0.33 and β of 0.8. The characteristic errors e_{ck} were stable at 146.58 mm with standard deviation of 18.38 mm for 3D and 2D sensor layouts when $\Delta L_{x, \max}$ was less than 1 m and increased enormously after the maximum sensor spacing was larger than 1 m with larger scatters among different

sensor layouts. This was due to the fact that direct waves through the crack could not be detected when the sensors are 1 m away from the actual source, but tip-diffracted waves were received instead. The arrival time delay of direct waves through the crack was measured to be within [5, 20] μs ,⁶ which caused a relatively stable source localization error, while tip-diffracted waves can introduce large time delays and consequently increase the errors. This observation suggested that e_{ck} were reasonably independent of the maximum sensor spacing when the spacing of the sensors is within the distance in which direct waves through the crack can be picked by the sensors (referred as allowable travel distance for direct waves). It is better to arrange sensors with maximum sensor spacing within the allowable travel distance for direct waves. This distance is

Table 2. Comparison of e_{ck} and $e_{ck,0.01}$ in test configuration 22.

Sensor layouts	Group 1		Group 2		Group 3			Group 4
	Type 1	Type 2	Type 3	Type 4	Type 5	Type 6	Type 7	Type 8
e_{ck} (mm)	160.35	172.76	115.95	116.62	117.04	130	150.33	55
$e_{ck,0.01}$ (mm)	193.91	214.24	142.13	144.22	141.42	156.21	186.82	65
$\frac{e_{ck,0.01} - e_{ck}}{e_{ck}}$ (%)	20.9	24	22.6	23.7	20.8	20.2	24.3	18.2

**Figure 8.** Cumulative distribution of source localization errors projected to the detection zone in sensor layouts: (a) Group 1, (b) Group 2, (c) Group 3, and (d) Group 4 in test configuration 22.

dependent on the attenuation properties of the material and the noise level during the test, thus requires additional calibrations.

The middle and right columns of Figure 9 show the influence of crack positions and crack height on e_{ck} , respectively, with $\Delta L_{x, \max}$ of 500 mm. They suggested

that e_{ck} is generally independent of the crack position. The e_{ck} increases with the crack height until a mean value of 147.06 mm with standard deviation of 16.61 mm among sensor layouts of 3D and 2D.

Experimental validation and discussion

An experimental validation of the simulated characteristic error was carried out on a reinforced concrete beam of size 10,000 mm \times 300 mm \times 1200 mm. The concrete had a nominal compressive strength of 65 MPa. The maximum aggregate size was 16 mm. Reinforcing bars in the beam were 6 ϕ 25, with concrete cover of 25 mm. The beam was simply supported with a span of 9 m and loaded by a point load in the mid-span, as schematically illustrated in Figure 10. The beam underwent a cyclic loading procedure as shown in Figure 11(a). The experimental validation was carried out when the beam was unloaded from a peak load of 250 kN (marked by an arrow in Figure 11(a)), thus the cracks were considered as relaxed, which complied with the assumed crack condition proposed in section “Wave propagation in concrete structures.” The crack pattern at the time of measurement is shown in Figure 12.

The wave speed and material attenuation in the tested concrete are the same as the modeled beam, being 4100 m/s and 20 dB/m at central frequency of 60 kHz, respectively. AE sensors with central frequency of 60 kHz were installed on the surface of the beam (x - z plane). The sensor spacing was 0.5 m. Sensors AE1, AE2, AE5, and AE6 enclosed detection zone 1 with dimension of $x \times z = 0.5 \text{ m} \times 0.5 \text{ m}$. Sensors AE2, AE3, AE6, and AE7 enclosed detection zone 2 with the same dimension, shown in Figure 12. Cracks in zone 1 and zone 2 had different local profiles and orientations. According to the definition in this article, the crack position factor α in zone 1 and zone 2 was around 0.21 (103/500) and 0.27 (133/500), respectively, and the crack height factor β was around 0.61 (306/500) and 0.68 (338/500), respectively.

In each zone, a grid of 10 \times 10 nodes was marked. In the lab tests, the AE signal source was generated by a 10-mm-diameter hammer hitting on the grid node. A typical hammer hit received by an AE sensor 5 cm away

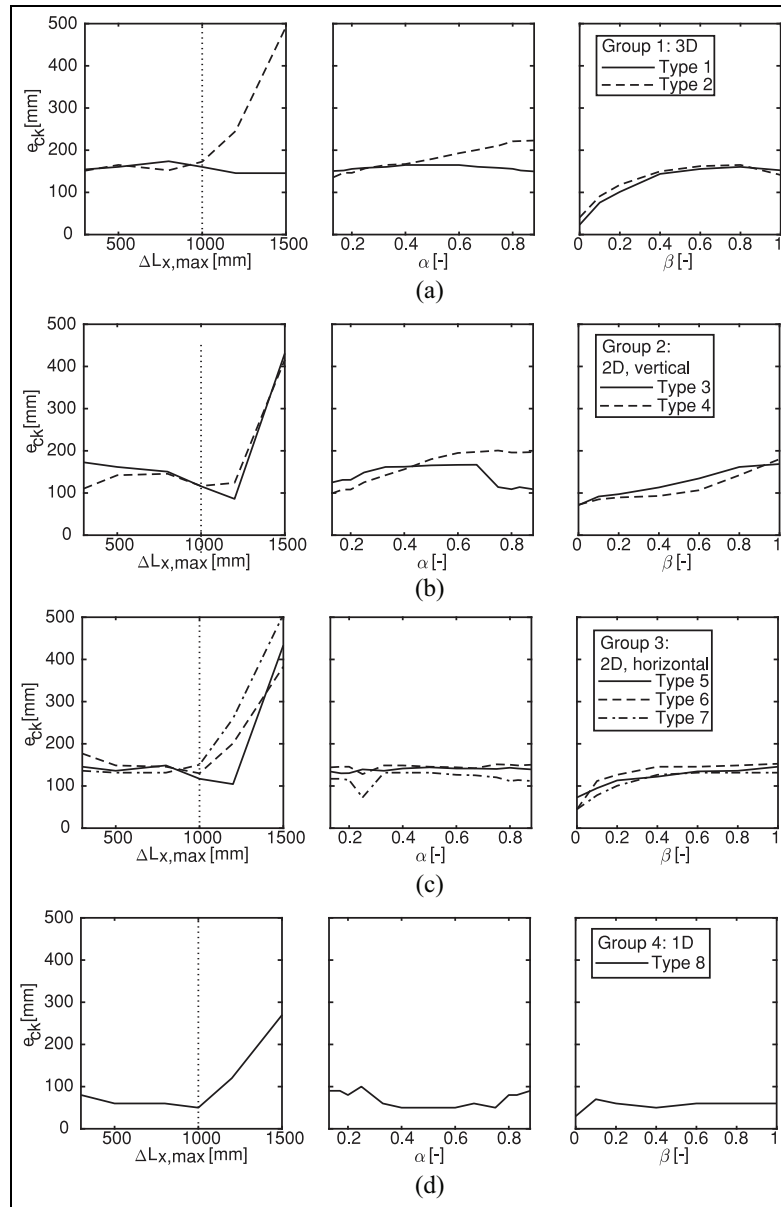


Figure 9. Characteristic source localization errors related to the maximum sensor spacing in x-direction $\Delta L_{x,max}$, crack position factor α , and crack height factor β in sensor layouts: (a) Group 1, (b) Group 2, (c) Group 3, and (d) Group 4.

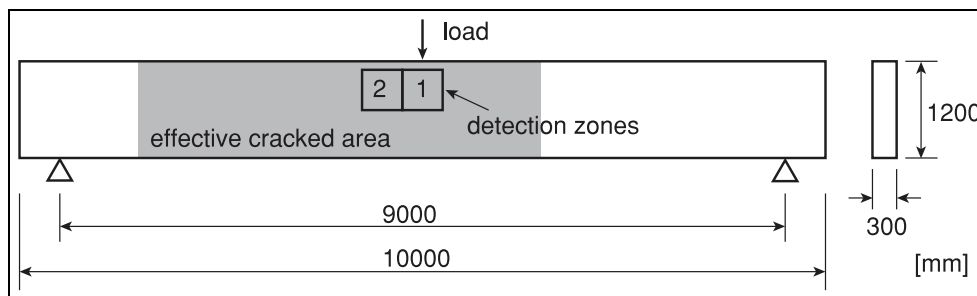


Figure 10. Dimension of the beam, detection zone, and load setup.

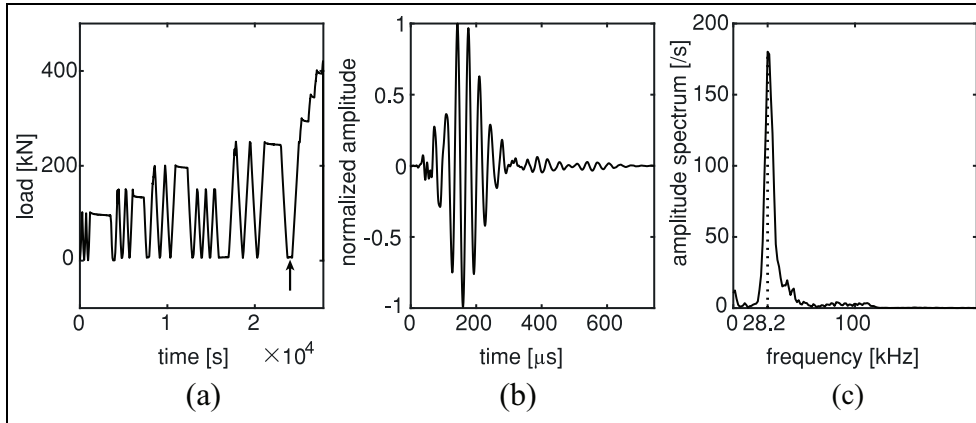


Figure 11. (a) Loading history with the time of measurement indicated by an arrow, (b) normalized hammer hit signal, and (c) amplitude spectrum of the normalized hammer hit signal.

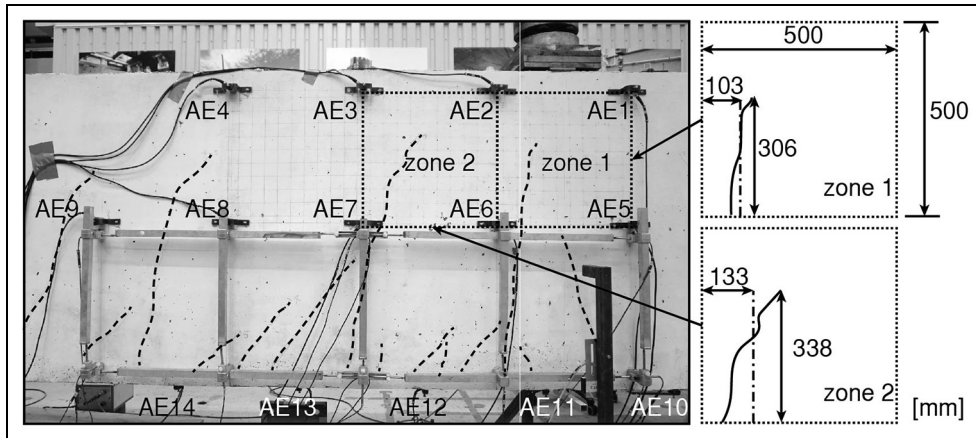


Figure 12. Experimental setup and crack pattern in the detection zones.

is shown in Figure 11(b). The received signal had a main frequency of 28.2 kHz (Figure 11(c)). A 2D source localization of the hammer hits was performed since the sources located inside the 2D detection zone. This was comparable to the 3D localization in the 3D detection zone (Group 1 in Figure 5) in the simulation, where the sources located inside the detection zone and no projection was needed.

The arrival times of each hammer hit at the four sensors in each zone was picked using the floating threshold crossing method to account the unstable amplitude of the hammer hits. The first point crossing 0.02 of the peak amplitude was picked as the first arrival, shown in Figure 13(a). The arrival time picking error in the shown case was around 5 μ s when compared to the manual pick. It should be noted that not all the picking errors in this validation test were within 5 μ s.

The grid search method outlined in section “AE source localization technique” was performed with a

grid searching zone of $x \times z = 0.9 \text{ m} \times 0.9 \text{ m}$. The source localization results in zone 1 are shown, for example, in Figure 13(b). The source localization results on the edge of the grid searching zone (in gray) were first filtered out. In zone 1 and zone 2, around 82% and 87% of the source localization results remained, respectively. The cumulative distribution of the remaining source localization results is presented in Figure 13(c). The characteristic localization error e_{ck} in zone 1 and zone 2 was 141.07 and 151.85 mm, respectively. From the simulation results shown in Figure 9(a), the characteristic error in the 3D layouts (Type 1 and Type 2) with $\Delta L_{x, \max}$ of 0.5 m and β of 0.6 was averaged at 158.85 mm (155.49 and 162.21 mm, respectively). The errors in the test zone 1 and test zone 2 were 11.2% and 4.4% less than the simulated errors, respectively. It indicated that some uncertainties of arrival time picking errors beyond 5 μ s in the source localization did not have a major impact on the characteristic source localization

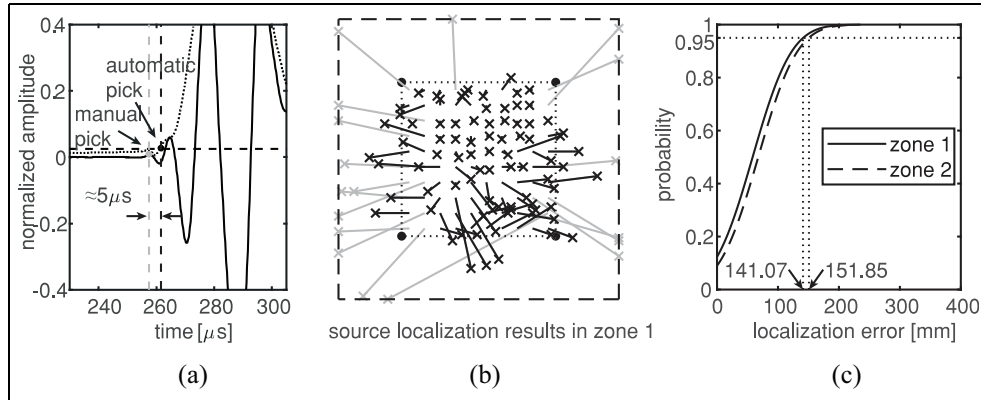


Figure 13. (a) Arrival time picking using the floating threshold crossing method, (b) source localization results in detection zone 1, and (c) cumulative source localization errors.

error. In addition, the fact that the e_{ck} evaluated from zone 1 and zone 2 was comparable suggested that the local profiles and the crack orientation had limited influence on the characteristic source localization error.

The experimental results gave a promising validation to the numerical model presented in this article, thus showing that the characteristic source localization error e_{ck} has the potential to be used as a reliable indicator to quantify the accuracy of source localization. In practical AE measurements, the information applied in the models, that is, the material properties, sensor layout, crack profiles, and arrival time picking errors, may vary. To implement the source localization model in practice, the following remarks are made:

- Before AE measurements, it is necessary to measure wave velocity, wave attenuation, and noise level in the concrete. The sensor spacing should be adjusted to allow the waves being received after attenuation;
- When multiple cracks exist between the source and the receiver, the influence of each crack on the attenuation of waves is expected to be summed up. This would result in less hits received or more late-arrived tip-diffracted waves;
- More sensors will improve the accuracy of source localization;
- The arrival time picking method is important for the source localization. In most acquisition systems, the implemented methods are based on the fixed or the floating threshold crossing. The floating threshold method applied in this study is suggested to be compared with the fixed threshold method with smaller time picking errors. A more accurate time picking method, Akaike information criterion (AIC),²⁰ shows a much smaller error around 1.25 μs .⁷ This would improve the source localization results.

Triangulation technique discussed in this article is a simplified method of AE source localization with many strong assumptions such as constant wave speed in concrete structures. For other improved methods which are also based on arrival times, such as those considering variable velocity distribution,^{11,12} the proposed evaluation approach and accuracy indicator can be used as well. In this way, the accuracy of AE source localization using different methods can be evaluated with a consistent approach. This could be an interesting future study.

Conclusion

This article focuses on quantifying the accuracy of AE source localization in concrete structures. A new methodology has been proposed, including a numerical algorithm to simulate the source localization process, a filtering criterion of the estimated AE location, and an indicator of source localization accuracy, namely characteristic error e_{ck} . The investigated influential factors include the location and height of a single crack, the random arrival time picking error, and the sensor layouts. Besides, the simulation result was further validated experimentally by comparing 100 AE sources generated by hammer hits with known locations on a cracked concrete beam. The following conclusions can be drawn:

- When grid search method was applied to do the source localization, the results at the edge of the grid searching zone were not sufficiently reliable and should be filtered out. Around 80% of the results remained afterwards in both the simulation and the validation tests with uniformly distributed sources in the detection zone;
- A term characteristic error e_{ck} was defined as the source localization error above which not more

than 5% of the total results are expected. In the simulated simplified situation, the expected characteristic error was 150 mm;

- The characteristic error e_{ck} was independent of the maximum sensor spacing when the maximum sensor spacing was within the allowable travel distance for direct waves;
- The characteristic error e_{ck} was independent of the crack position in the detection zone but reduced with the reduction in the crack height when a single crack is present in the detection zone;
- The experimental validation suggests that the proposed evaluation approach and indicator of the accuracy of the source localization are reliable. To apply the characteristic source localization error obtained in this article in other applications, the inputs, like the material properties, sensor layout, and the crack pattern of the structure, should be first justified. In case of significant deviation, the proposed method should be adjusted accordingly.


Declaration of conflicting interests

The author(s) declared no potential conflicts of interest with respect to the research, authorship, and/or publication of this article.

Funding

The author(s) received no financial support for the research, authorship, and/or publication of this article.

ORCID iD

Fengqiao Zhang  <https://orcid.org/0000-0001-9025-3252>

References

1. Ohtsu M, Uchida M, Okamoto T, et al. Damage assessment of reinforced concrete beams qualified by acoustic emission. *ACI Struct J* 2002; 99: 411–417.
2. Zhang F and Yang Y. Acoustic emission based crack tracking for existing concrete structural members. In: *9th international conference on acoustic emission*, Chicago, IL, 17–20 June 2019.
3. Yang Y, Hordijk DA and de Boer A. Acoustic emission study on 50 years old reinforced concrete beams under bending and shear tests. In: *8th international conference on acoustic emission*, Kyoto, Japan, 5–9 December 2016.
4. Grosse CU and Ohtsu M. *Acoustic emission testing: basics for research-applications in civil engineering*. Berlin: Springer, 2008, 404 pp.
5. Miller RK, Pollock AA, Watts DJ, et al. A reference standard for the development of acoustic emission pipeline leak detection techniques. *NDT&E Int* 1999; 32: 1–8.
6. Pahlavan PL, Zhang F, Yang Y, et al. Interaction of ultrasonic waves with partially-closed cracks in concrete structures. *Constr Build Mater* 2018; 167: 899–906.
7. Schechinger B and Vogel T. Acoustic emission for monitoring a reinforced concrete beam subject to four-point-bending. *Constr Build Mater* 2007; 21: 483–490.
8. Tsangouri E, Karaiskos G, Deraemaeker A, et al. Assessment of acoustic emission localization accuracy on damaged and healed concrete. *Constr Build Mater* 2016; 129: 163–171.
9. Zhang F. *Evaluation of acoustic emission monitoring of existing concrete structures*. Master's thesis, Delft University of Technology, Delft, 2017.
10. Kundu T. Acoustic source localization. *Ultrasonics* 2014; 54: 25–38.
11. Shiotani T, Osawa S, Momoki S, et al. Visualization of damage in RC bridge deck for bullet trains with AE tomography. In: Shen G, Wu Z and Zhang J (eds) *Advances in acoustic emission technology*. New York: Springer, 2015, pp. 357–368.
12. Pahlavan P, Paulissen J, Pijpers R, et al. Acoustic emission health monitoring of steel bridges, 2014, <https://hal.inria.fr/hal-01021221/document>
13. Ohtsu M. Recommendation of RILEM TC 212-ACD: acoustic emission and related NDE techniques for crack detection and damage evaluation in concrete—measurement method for acoustic emission signals in concrete. *Mater Struct* 2010; 43: 1177–1181.
14. MISTRAS Group Inc. *AEwin Software, installation, operation and user's reference manual*. Princeton, NJ: Products & Systems Division, MISTRAS Group Inc, 2011.
15. Philippidis TP and Aggelis DG. Experimental study of wave dispersion and attenuation in concrete. *Ultrasonics* 2005; 43: 584–595.
16. Ogilvy JA and Temple JAG. Diffraction of elastic waves by cracks: application to time-of-flight inspection. *Ultrasonics* 1983; 21: 259–269.
17. Zhang F, Pahlavan PL, Yang Y, et al. Influence of cracks on the reliability of acoustic emission monitoring of concrete structures. In: *2nd international RILEM/COST conference on early age cracking and serviceability in cement-based materials and structures*, Brussel, 12–14 September 2017.
18. EN 1992-1-1:2004. Eurocode 2: Design of concrete structures—General rules and rules for buildings.
19. Hogg RV, McKean JW and Craig AT. *Introduction to mathematical statistics*. London: Pearson, 2019.
20. Kurz JH, Grosse CU and Reinhardt H-W. Strategies for reliable automatic onset time picking of acoustic emissions and of ultrasound signals in concrete. *Ultrasonics* 2005; 43: 538–546.